Talanta 222 (2021) 121466

Contents lists available at ScienceDirect

Talanta

journal homepage: www.elsevier.com/locate/talanta

Investigation of the recognition interaction between glycated hemoglobin and its aptamer by using surface plasmon resonance

Dapeng Sun [a,b], Yi Wu [c], Shwu-Jen Chang [d], Ching-Jung Chen [a,e,*], Jen-Tsai Liu [a,f,**]

[a] Research Center for Materials Science and Opti-Electronic Technology, University of Chinese Academy of Sciences, No.19A Yuquan Road, Beijing, 100049, PR China
[b] School of Electronic, Electrical and Communication Engineering, University of Chinese Academy of Sciences, PR China
[c] School of Physics, University of Chinese Academy of Sciences, PR China
[d] Department of Biomedical Engineering, I-Shou University, Kaohsiung City, 82445, Taiwan
[e] School of Opto-Electronic Technology, University of Chinese Academy of Sciences, PR China
[f] College of Materials Science and Opto-Electronic Technology, University of Chinese Academy of Sciences, PR China

ARTICLE INFO

Keywords:
HbA1c
Aptamer
SPR
Recognition interaction

ABSTRACT

Glycated hemoglobin (HbA1c) has been widely explored as an important marker for monitoring and diagnosing diabetes. Due to the advantages of high selectivity, easy preparation, and convenient preservation of aptamers, research on glycated hemoglobin detection utilizing aptasensors has received much attention in recent years. However, factors such as the pH and the salt concentration of the solution and the structure of the aptamer could influence the interactions between HbA1c and the aptamer. In this study, the factors were evaluated using surface plasmon resonance (SPR). The results show that the pH and the salt concentration can greatly affect the formation of a complex between the aptamer and HbA1c. In the stereostructure of the aptamer, loop L1 may be an important motif for recognizing glycated hemoglobin. In addition, the best condition for detecting HbA1c was at pH 6, with a high sensitivity and a low limit of detection(LOD) (1.06×10^{-3} $\frac{RU}{nM}$ /2.55 nM). The results also demonstrated that the use of an SPR aptamer biosensor can be a sensitive technique to improve the accuracy and correctness of HbA1c measurement.

1. Introduction

Diabetes mellitus is one of the most common noncommunicable diseases in the world. Statistics show that there were approximately 382 million people suffering from diabetes in 2013, and the number of diabetes cases is growing fast and predicted to reach 592 million by 2035 [1]. Diabetes can lead to blindness, leg amputations, nontraumatic foot disorders, acute complications and even death [2]. However, evidence has shown that early diagnosis and strict control of glucose levels can prevent or delay diabetes-related complications [3]. Increasing glucose levels are one of the criteria for diabetes diagnosis, but they are also affected by stress, exercise and many other factors. Compared with the glucose level, the glycated hemoglobin (HbA1c) content reflects the average concentration of glucose for the most recent 2–3 months, which is attributed to the life span of red blood cells of 100–120 days [4]. Therefore, for long-term glycemic control of diabetes and evaluation of related complications, the HbA1c ratio is an important clinical index.

HbA1c measurement methods include high-performance liquid chromatography (HPLC), enzyme-linked immunosorbent assays (ELISAs), fluorescence sensing, chromatography and immunoturbidity assays [5]. However, there are many disadvantages among these methods. The HPLC method has been used as the gold standard for HbA1c measurement, though large and expensive equipment is required. For immunoassay-based methods, antibodies are necessary, which are expensive and unstable for long-term storage. For fluorescence sensing, labeling may affect the adsorption behavior of proteins and probes. In recent years, an alternative method of detecting HbA1c has involved using HbA1c-specific aptamers. Aptamers are a class of oligonucleotide or peptide molecules that can discriminate target molecules on the basis of subtle structural differences. Compared with antibodies, aptamers have the advantages of customization, extremely accurate chemical synthesis, no batch variation, reproducibility, reversible denaturation

* Corresponding author. No.19A Yuquan Road, Beijing, 100049, PR China.
** Corresponding author. Research Center for Materials Science and Opti-Electronic Technology, University of Chinese Academy of Sciences, No.19A Yuquan Road, Beijing, 100049, PR China.
E-mail addresses: cjchen@ucas.ac.cn (C.-J. Chen), jtliu@ucas.ac.cn (J.-T. Liu).

https://doi.org/10.1016/j.talanta.2020.121466
Received 7 May 2020; Received in revised form 25 July 2020; Accepted 26 July 2020
Available online 2 August 2020
0039-9140/© 2020 Elsevier B.V. All rights reserved.

and long-term storage. Most importantly, aptamers are non-immunogenic [6], so it will be better to simulate their application in the human blood environment.

HbA1c-specific aptamers were first prepared by Lin et al. They used systematic evolution of ligands by exponential enrichment (SELEX) through an in vitro process to obtain HbA1c aptamers. The specificity and affinity of the aptamers were computed, along with the dissociation constant for HbA1c, which was Kd = 7.3 ± 2.2 nM [7]. However, Kimoto et al. [8] reported that too much tedious modification of DNA and the test substance can affect the affinity and original shape of the aptamer. Therefore, using the original aptamer with few modifications to catch the target is the best way to maintain high affinity for detection.

Surface plasmon resonance (SPR) is a surface-sensitive optical technique that is used for the determination of analytes. This approach can detect the thickness of films adsorbed onto the sensor surface and interactions between biomolecules such as antigen-antibody or protein-DNA interactions. In comparison with traditional detection methods such as X-ray, HPLC, High Performance Liquid Chromatography-Mass Spe (HPLC-MS), etc. SPR technique not only is a label-free and rapid detection method but also allows kinetic parameter measurements (of association and dissociation processes), concentration measurements and real-time molecule detection [9]. More importantly, the SPR technique is an excellent detection method for real-time on-line analysis of molecular dynamics. Therefore, an increasing number of researchers have recently begun to use SPR to study the structure of aptamers to capture target analytes. He et al. used SPR to observe anti-recombinant human erythropoietin α aptamers with different sequences [10]. By designing different stem and loop designs, the aptamer with the best affinity was found, which confirmed that the structure of the aptamer affects its affinity with the test substance. Wang, S. et al. [11] achieved better conformational folding and better accessibility to small molecules for aptamers by designing a more uniform graft base, which validated that the electrostatic force around the pre-interfering aptamer can promote the formation of a better structural shape (in terms of spatial structure) so that the aptamer can grasp the object to be detected. Wochner et al. [12] designed an aptamer with different secondary structures based on the original aptamer through mfold and identified a high affinity daunomycin aptamer with strong resistance to environmental interference through SPR, which put forward the view that the factors affecting the affinity between the aptamer and the detection object, in addition to the structure of the aptamer, are also affected by the environmental pH and the electrostatic shielding of sodium salts.

Many studies have used aptamers to specifically capture glycated hemoglobin. Among the published articles, there are two effective HbA1c aptamers [13,14], the most cited of which was reported by Chang et al. in 2015. However, these works have not explored the concrete reason for the interaction between aptamers and target proteins [7,15–18]. In addition, these studies use the sandwich method with a long incubation time to obtain experimental data, which prevents samples from being quickly detected in medical applications within the validity period. To the best our knowledge, this is the first study to investigate the interaction between an aptamer and HbA1c by using SPR, in which the interaction is changed by the pH and the salt concentration of the buffer as well as the structure of the aptamer. Beside, SPR technique is a direct detection method without any incubation which can provide a valuable reference for fast detect HbA1c in medical diagnosis.

2. Materials and method

2.1. Reagents

DNA sequences were purchased from Sangon Biotech. Ltd. (Shanghai, China). Bovine albumin (BSA) was purchased from Sigma-Aldrich Company Ltd. (USA). Glycated hemoglobin was purchased from ProSpec-Tany TechnoGene Ltd. (Ness Ziona Israel). 8-Thiooctanoic acid (MOA) was purchased from Sigma-Aldrich Company Ltd. (USA). N-Hydroxysulfosuccinimide sodium salt (sulfo-NHS), 1-(3-dimethylaminopropyl)-3-ethylcarbodiimide hydrochloride (EDC) and 6-mercapto-hexan-1-ol (MCH) were purchased from Aladdin Chemistry Co. Ltd. (Shanghai, China). Sodium dodecyl sulfate (SDS) was obtained from Beijing Biotopped Science & Technology Co. Ltd. (Beijing, China). Absolute ethyl alcohol, $Na_2HPO_4{\cdot}12H_2O$, $NaH_2PO_4{\cdot}2H_2O$ and NaCl were purchased from Beijing Chemical Works (Beijing, China). 2-Morpholinoethanesulfonic acid (MES) was purchased from Shanghai Macklin Biochemical Co. Ltd. (Shanghai, China). Deionized water obtained from a Millipore Direct-Q 5UV water purification system was used in all experiments. Matching oil series E (1.520) was purchased from Cargill Dow LLC. (USA). According to the study of HbA1c [19], the experimental environment was set to a pH of 6.96, at the isoelectric point of HbA1c, a pH of 7.4, above the isoelectric point of HbA1c, and a pH of 6, below the isoelectric point of HbA1c, forming an environment that makes the protein uncharged, negatively charged and positively charged, respectively. Four kinds of binding buffers were used in this study: (1) 0.1 M phosphate buffer (PB) with sodium chloride (137 mM) at pH 7.4. (2) 0.1 M PB without sodium chloride at pH 7.4. (3) 0.1 M PB without sodium chloride at pH 6. (4) 0.1 M PB without sodium chloride at pH 6.96.

2.2. SPR testing equipment

To more intuitively observe the adsorption behavior and kinetic relationship between aptamers and analytes, we use the most representative SPR instrument as the detection device. The self-developed SPR machine consisted of a temperature control component, mechanical motion detection component, microchannels, and host computer parts. The mechanical motion detection part mainly consisted of two mechanical arms that can move together, which are separately mounted on a 650 nm laser with a P polarizer and a photodetector. The movement of the robot arm is driven by a precision turntable so that the robot arm can be precisely controlled. The temperature control part is controlled by PWM waves to adjust the thermoelectric coolers, which maintain a stable temperature ±0.03 °C. The main body of the microchannel part is made of stainless steel. Due to its good thermal conductivity, oxidation resistance, and structural strength, this part can serve as a temperature-control medium while facilitating sample trace transfers, and it does not clog easily. Finally, the main function of the host computer is to set the rotation angle of the robot arm and collect the light intensity signal and process the collected signal to obtain the entire SPR curve. We added acceleration and deceleration processes in the control algorithm to drive the motors, which greatly increase the accuracy of our control of the robotic arm to ensure that the best resonance angle is obtained. In addition, we chose the main control chip STM32ZET6 for stable data acquisition and fast data transmission, which integrated a high-precision analog-to-digital converter and operating frequency. The home-made SPR system [20] has a refractive index resolution of 2.46×10^{-6} refractive index units (RIUs) and a wide dynamic range of 40°–72°, providing valid experimental data for research work.

2.3. Simulation and selection of aptamers

'mfold' is simulation software for predicting the secondary structure of single-stranded nucleic acids. Through this simulation software, researchers can quickly and freely obtain the secondary structure of ssDNA designed by themselves under the conditions that they set [21]. Therefore, we can observe the changes in aptamer structure under different parameters, and these conditions are known and controllable.

In this study, the glycated hemoglobin aptamer [7], which has been cited many times, is used as the original chain. The aptamer sequences is showed as Table 1. Through the simulation, we obtained a stable secondary structure under experimental conditions. As shown in Fig. S1(a), we divided three loops from this basis (L1, L2, and L3) and designed

Table 1
Glycated hemoglobin aptamer base sequences.

Sequence number	Sequences
Aptamer0	5′-GGC AGG AAG ACA AAC ACA TCG TCG CGG CCT TAG GAG GGG CGG ACG GGG GGG GGC GTT GGT CTG TGG TGC TGT-3′
	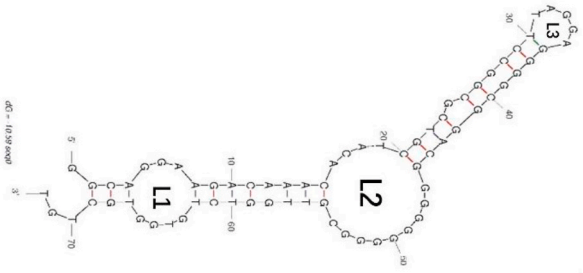
Aptamer1	5′-GGC ACG CAG ACA AAC ACA TCG TCG CGG CCTTAG GAG GGG CGG ACG GGG GGG GGC GTT GGT CTG TG TGC TGT-3′
	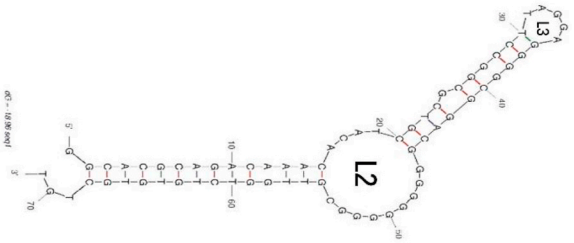
Aptamer2	5′-GGC AGG AAG ACA AAC ACA TCG TCG CGG CCT TAG GAG GGG CGG ACG ATG T GTT GGT CTG TGG TGC TGT-3′
	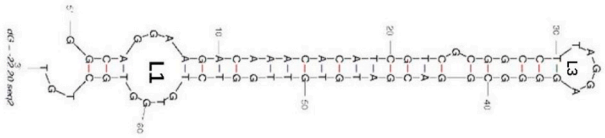
Aptamer3	5′-GGC AGG AAG ACA AAC ACA TCG TCG CGG CCT TAG GGC GGA CGG GGG GGG GCG TTG GTC TGT GGT GCT GT-3′
	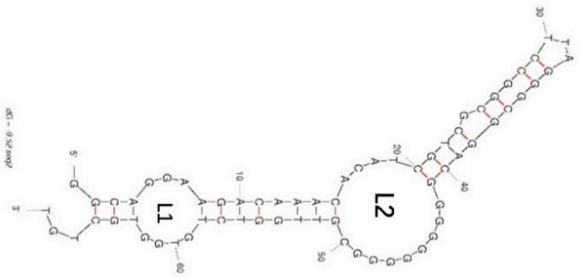

three other aptamers (Fig. S1(b)–(d)) to investigate the effect of DNA structure on the specific binding of target proteins. To facilitate grafting, we purchased aptamers that modified the amino group at the 3′ end of the synthetic DNA.

2.4. Sensor modification and characterization

For HbA1c detection, we need to modify the sensor with aptamers. Fig. 1 is the scheme of the sensor modification process. The sensor chip

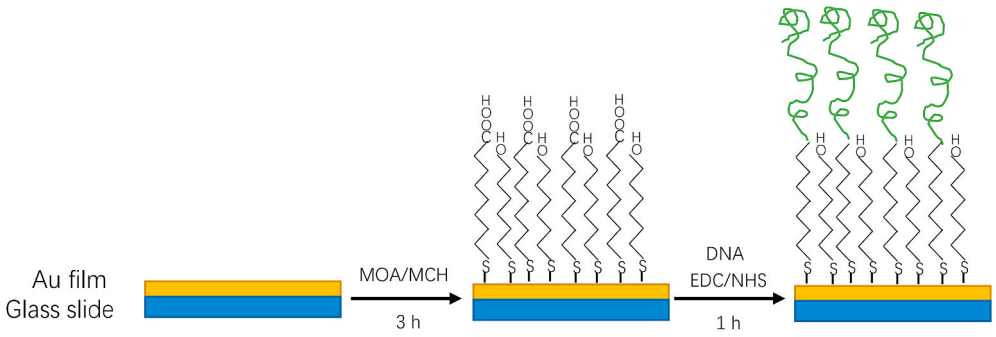

Fig. 1. Scheme of the sensor modification process.

was first washed with absolute ethanol and exposed to UV light for 30 min. The sensor chip was immersed in 10 mM MCH and 2 mM MOA (5:1) for 3 h at 25 °C. We chose the mixed membrane of MOA and MCH because of the similar length of the two mercapto chains. In this way, when forming a self-assembled monomolecular layer dominated by hydrogen bonds between MOA and MCH, the layer will be relatively uniform, and long-chain molecules are less prone to clumping. In addition, the length of MOA with –COOH is slightly longer than that of MCH with –OH, which is convenient for grafting with DNA modified evenly with amino groups for reasonable distribution [22]. After rinsing with absolute ethyl alcohol, the solution was incubated in 1 μM DNA solution with 5 mM EDC and 5 mM NHS dissolved in 0.1 M MES (pH = 5.5) for 1 h [20]. Finally, the sensor chip was washed with deionized water, dried with nitrogen and stored at 6 °C.

To observe and characterize the sulfhydryl groups and DNA on the modified gold film, we performed water contact angle measurements and X-ray photoelectron spectroscopy (XPS) at different stages to ensure that successful modification occurred at each stage.

2.5. Antifouling performance test

The sensor chip's specificity to a given analyte has a crucial effect on the experimental measurements. However, depending on the surface properties, nonspecific adsorption of proteins may be caused by hydrogen bonding, electrostatic, charge-transfer, and hydrophobic interactions [23]. The BSA protein contains hydrophobic, hydrophilic, cationic and anionic regions and is suitable for checking the specificity of the probe [24–26]. Therefore, the current experiment used 147 nM HbA1c as a control group and two BSA concentrations (149 nM and 149 mM) to evaluate the nonspecific adsorption of the sensor.

2.6. SPR measurement

To observe the binding phenomenon of HbA1c and aptamer and analyze the kinetic parameters between them, SPR was used to test the adsorption of HbA1c at different concentrations (294 nM, 220 nM, 147 nM, and 73 nM) in different buffer environments (0.1 M PB/pH = 7.4, 0.1 M PB/pH = 6.96, 0.1 M PB/pH = 6, and 0.1 M PB+137 mM NaCl/pH = 7.4). All experiments were based on the self-developed SPR setup. The experiment temperature was set at 25 °C, consistent with the temperature conditions simulated by mfold.

First, the sensor chip was placed in the instrument, and the buffer solution was injected at a flow rate of 50 μl/min for 1 h. After obtaining a stable test baseline, the HbA1c solution was flowed for 30 min to obtain the adsorption curve, and then, the buffer solution was further flowed for 30 min to obtain a desorption curve. It is necessary to rinse the pipeline with 0.1% SDS for 60 min and deionized water for 120 min after finishing the work.

2.7. Kinetic calculations

The research theory used in this research is Langmuir isotherm adsorption model theory. In the binding process, HbA1c, aptamer and conjugate were regarded as analyte A, ligand B, and complex AB, respectively. The experimental data were fitted with a 1:1 interaction model, and the whole process can be expressed by Equation (1).

$$[A] + [B] = [AB] \tag{1}$$

Affinity interactions between A and B were defined by the association rate constant ka and dissociation rate constant kd, and they have the following relationship [4].

$$k_a \cdot [A] \cdot [B] = k_d \cdot [AB] \tag{2}$$

The equilibrium association constant $K_D = \frac{k_d}{k_a}$, and the affinity constant $K_A = \frac{1}{k_D}$.

During the association period, [AB] has the following relational expression.

$$\frac{d[AB]}{dt} = k_a \cdot [B] \cdot [A] - k_d \cdot [AB] \tag{3}$$

During the reaction at time t, [B] = $[B]_0$- [AB], where $[B]_0$ is the initial ligand concentration. Then, Equation (3) was converted to Equation (4).

$$\frac{d[AB]}{dt} = k_a \cdot [A] \cdot ([B]_0 - [AB]) - k_d \cdot [AB] \tag{4}$$

Equation (4) is solved to yield equation (5).

$$\frac{[AB]}{[B]_0} = \frac{[A]}{[A] + \frac{k_d}{k_a}} \cdot [1 - e^{-(ka[A] + kd)t}] \tag{5}$$

ks is defined as the apparent reaction rate constant and has the expression shown in Equation (6).

$$k_s = k_a \cdot [A] + k_d \tag{6}$$

In the SPR system, the response value R has a linear relationship with AB, and [AB] can be replaced by R. After completing the saturation experiment, [AB] = $[B]_0$, and the maximum response value R_{max} is obtained ($R_{max} = [B]_0$). Then, Equation (7) evolves from Equation (4).

$$\frac{R}{R_{max}} = \frac{ka \cdot [A]}{ka \cdot [A] + kd} [1 - e^{-(ka[A] + kd)t} \tag{7}$$

$\frac{R_{max} \cdot k_a \cdot [A]}{k_a \cdot [A] + k_d}$ is replaced by R_e,

$$R = R_e [1 - e^{-k_s \cdot t}] \tag{8}$$

The data of the SPR adsorption curves at different concentrations of A are fitted with Equation (8) to obtain the ks values of the corresponding concentrations [20].

$$\begin{cases} ks_1 = ka[A]_1 + kd \\ ks_2 = ka[A]_2 + kd \\ ks_i = ka[A]_i + kd \end{cases} \tag{9}$$

where i is the analyte concentration.

Finally, the fitting line is made according to [A] with different concentrations and k_s corresponding to [A] to obtain the slope k_a, the intercept k_d, and K_A.

3. Results and discussion

3.1. Characterization of successful sensor modification

To understand the surface characteristics of every modification process, we used the water contact angle and XPS to verify the successful grafting on the Au surface (Fig. 2). For the freshly plated film, we measured a bare gold contact angle of 55.5 ± 2° [27]. The contact angle of bare Au after UV cleaning was barely detectable (almost 0°). After forming the MOA-MCH mixed self-assembled monolayer (SAM), the contact angle changed from 0° to 23 ± 2°. This change was attributed to the hydroxyl and carboxyl functional groups, which are more hydrophilic than the bare Au surface [28]. Interestingly, the contact angle decreased to 13 ± 2° after DNA immobilization. This increase in hydrophilicity was due to the hydrophilic nature of phosphoric acid, indicating the successful immobilization of DNA onto the mixed SAM/Au [29].

As shown in Fig. 3, only the element gold was present on the chip without surface modification. The core-level spectra of the MOA/MCH stage are presented in Fig. S2. The C1s spectrum (Fig. S2(a)) shows that the peaks at 284.8 eV, 286.4 eV, and 289.1 eV should be attributed to C–C, C–OH and O═C–OH, respectively. Three distinct peaks at 531, 532.3 and 533.3 eV in the O1s spectrum (Fig. S2(b)) represent the

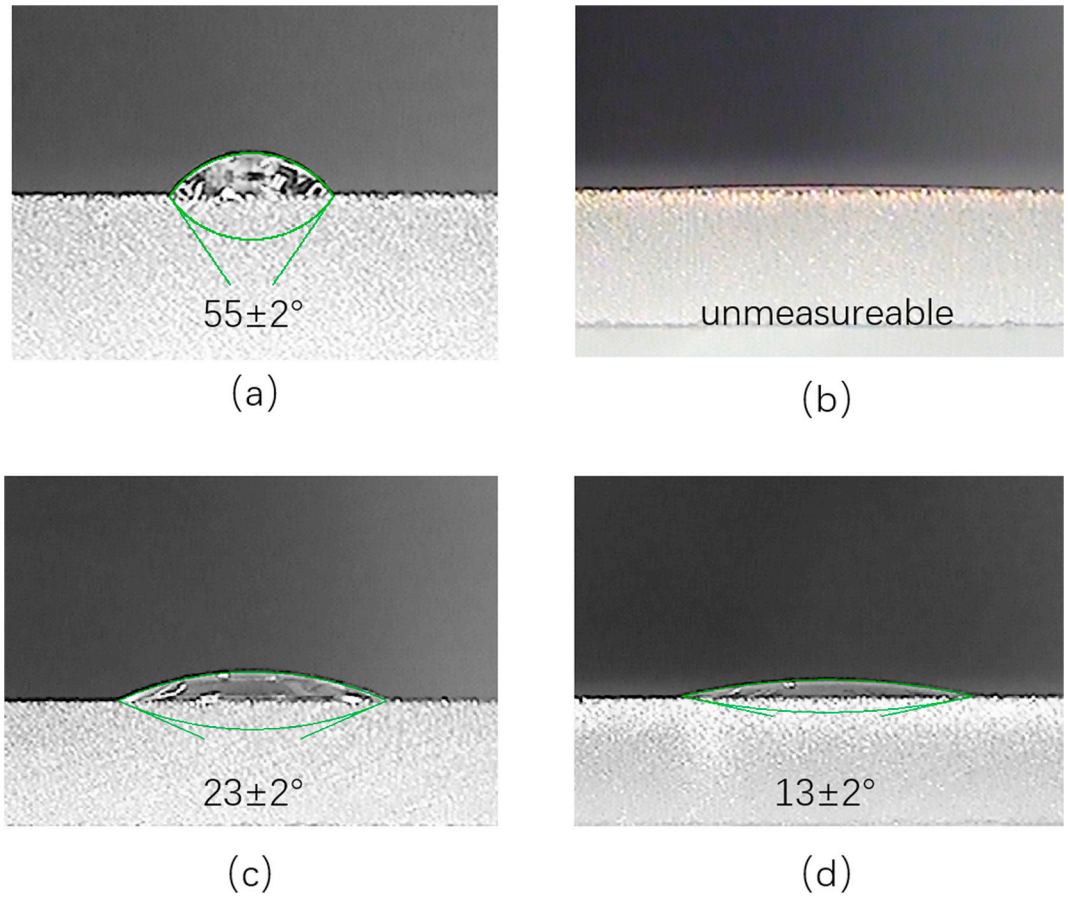

Fig. 2. Contact angle measurement of (a) bare Au, (b) bare Au after UV exposure, (c) Au/MOA/MCH SAM, and (d) Au/MOA/MCH/aptamer.

presence of C═O, C–OH and O–C–O, respectively. This result is due to the exposed –COOH and –OH groups of MOA and MCH, respectively. The high binding energy peak at 162.5 eV and low binding energy peak at 166.5 eV were attributed to Au–S and $–SO_3$, respectively (Fig. S2(c)). This result showed that most of the MOA/MCH molecules were bonded to Au by Au–S linkages, and only a small amount of S was oxidized.

In the MOA/MCH/aptamer stage, the spectrum of N1s (Fig. S3(b) shows that amines ($C–NH_2$) and amides (O = C–NH) appear at 400 eV and 401.5 eV, respectively. These peaks are observed because the amino group on the DNA and the carboxyl group at the end of MOA are dehydrated and condense to form an amide, and the DNA is rich in nitrogen bases and grafted onto the SAM. The P2p spectrum (Fig. S3(d)) showed that the P element peak appeared at 133.4 eV, which was caused by DNA containing phosphate backbones (see Table 1).

Assuming that the theoretical grafting value is 100%, each grafted DNA molecule has approximately 70 phosphate groups (P), and one DNA molecule corresponds to 6 thiol groups (MCH: MOA = 5:1). Therefore, according to the element content in Table 2, we can roughly calculate the grafting rate of DNA as 5%. The above data demonstrate that the SAM and DNA are successfully immobilized on the gold surface.

3.2. Antifouling performance

BSA is very easy to adhere to the surface of the material and can be used as a contaminant to conduct antifouling performance experiments [30]. Fig. 4 shows the response curves for the three samples. BSA (149 nM) was used to test the sensor's antifouling performance, and it was found that the SPR signal value was almost unchanged. BSA (149 mM) was used to verify the antifouling properties at physiological environmental concentrations, and the results increased to 0.015 RU. The response value of 147 nM HbA1c is more than 10 times that of 149 nM BSA. This finding showed that the recognition layer had good antifouling performance. Otherwise, compared with 0.085 RU of the control group (147 nM HbA1c), the results showed that the sensor has high specificity. The above data show that the aptamer identification layer has high antifouling performance and specificity.

3.3. The results of SPR measurements

The experimental tests used four types of buffers and aptamers. To facilitate comparison of the results under different conditions, all experimental response plots are divided, as shown in Figs. 5 and 6, Figs. S4 and S5. Fig. 5 shows the response of aptamer0 in different buffer environments. Under the conditions of pH = 6/0.1 M PB, pH = 6.96/0.1 M PB, pH = 7.4/0.1 M PB and pH = 7.4/0.1 M PB + 137 mM, the sensitivity and LOD are $1.06 \times 10^{-3}\frac{RU}{nM}$/2.55 nM, $3.885 \times 10^{-4}\frac{RU}{nM}$/6.95 nM, $5.763 \times 10^{-4}\frac{RU}{nM}$/4.68 nM and $7.4 \times 10^{-5}\frac{RU}{nM}$/36.48 nM, respectively. The results show that pH 6/0.1 M PB is the best detection condition and the linear range is 73 nM–294 nM. Under this condition, the coefficient of determination is higher than 0.98. Compared with the condition of pH = 7.4/0.1 M PB + 137 mM, the sensitivity of the pH 6/0.1 M PB condition is increased by 2 orders of magnitude; in terms of LOD, it is decreased by one order of magnitude. This result shows that changes in the pH and the salt concentration can greatly affect the forces between the aptamer and HbA1c. The results show that the optimal test environment is inconsistent with that of many current studies [7,15,18,31–33], which indicates that more than one factor can influence the interaction between aptamer0 and HbA1C.

In Fig. S4, the adsorption characteristics of aptamers with different structures and HbA1c in the same buffer (pH = 7.4/0.1 M PB) are shown. Under the conditions of aptamer0, aptamer1, aptamer2 and aptamer3,

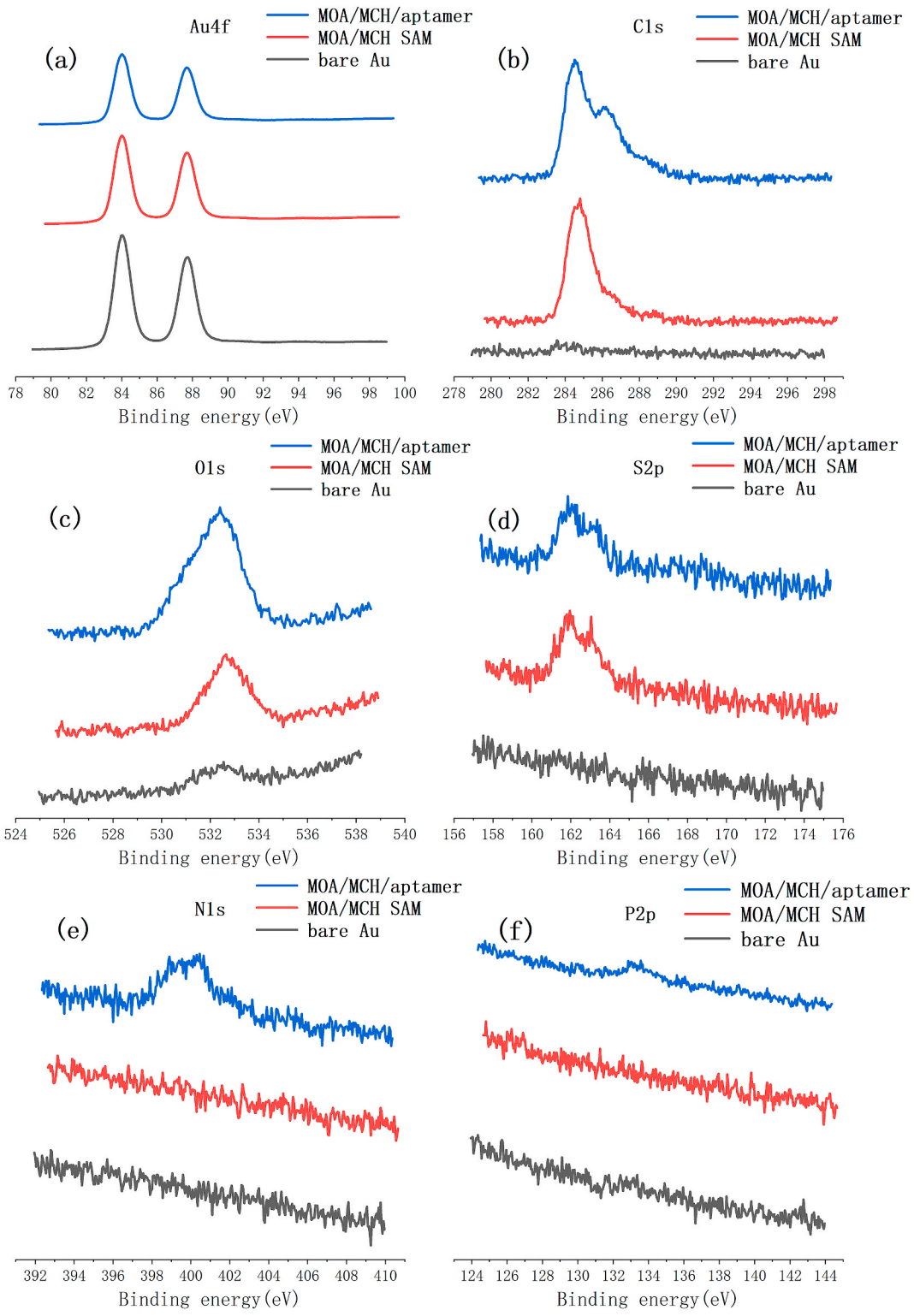

Fig. 3. XPS spectra of the sensor in different processes: (a) Au, (b) carbon, (C) oxygen, (d) sulfur, (e) nitrogen, (f) phosphorus line, where the black, red and blue lines represent the stages of bare Au, Au/mixed SAM and Au/mixed SAM/aptamer, respectively. (For interpretation of the references to colour in this figure legend, the reader is referred to the Web version of this article.)

the sensitivity and LOD are 5.763×10^{-4} $\frac{RU}{nM}$/4.68 nM, 5.38×10^{-4} $\frac{RU}{nM}$/5.02 nM, 1.834×10^{-4} $\frac{RU}{nM}$/14.72 nM and 1.154×10^{-4} $\frac{RU}{nM}$/23.35 nM, respectively. The results show that aptamer0 is the optimal detection condition. Compared with that of the aptamer3 conditions, the sensitivity of aptamer0 is increased by 4 times; in terms of LOD, it is decreased by one order of magnitude. This result illustrates that differences in the structure of the aptamer will affect its interaction with HbA1c.

From the above measurement data, it can be concluded that the change in pH has a higher impact on aptamers and HbA1c. This result is likely because the combination of aptamers and analytes is promoted and the aptamer structure forms better binding sites on a three-

Table 2
XPS results of elemental percentages.

Modification process	Au4f (Atomic %)	S2p (Atomic %)	C1s (Atomic %)	O1s (Atomic %)	N1s (Atomic %)	P2p (Atomic %)
Bare Au	100	0	0	0	0	0
Au/mixed SAM	53.71	5.06	34.36	6.87	0	0
Au/mixed SAM/aptamer	35.23	4.52	37.43	11.33	9	2.49

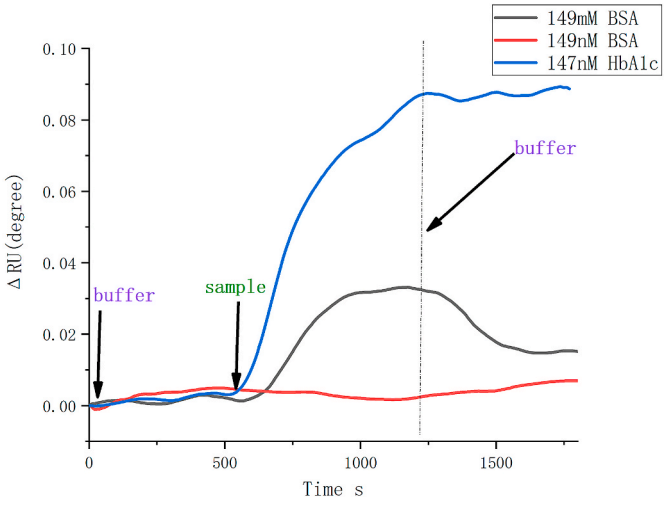

Fig. 4. SPR response of the aptasensor with BSA and HbA1c.

dimensional structure at pH = 6. Under the condition of pH = 6, the aptamer is negatively charged and glycated hemoglobin is positively charged. The interaction between the two is promoted by electrostatic attraction, which makes the response signal larger.

3.4. SPR kinetic parameters

In Langmuir isotherm adsorption model, the interaction process of HbA1c and aptamer was divided into association and disassociation phases, and the obtained kinetic parameters for the phases are listed in Table 3.

Combining the response diagrams and kinetic parameter results of four concentrations of the test substance under different conditions, we obtain that aptamer1 possesses a maximum k_a (8.78×10^4 M^{-1} s^{-1}) at pH = 7.4/0.1 M PB, which is due to truncation of the L1 loop on the aptamer. Comparing all the experimental conditions and kinetic data, we screened out the conditions that gave the maximum K_A: pH = 6 and 0.1 M PB. The data showed that under the condition of pH = 6/0.1 M PB, there is a strong binding behavior between HbA1c and aptamer.

3.5. Analysis of the interaction between aptamer and glycated hemoglobin

3.5.1. Effect of electrostatic force

It is generally believed that any changes or chemical reactions that occur in independent systems always proceed in the direction of decreasing enthalpy (ΔH <0) and increasing entropy (ΔS> 0). Therefore, the process of binding aptamers and proteins into complexes is spontaneous, which can be explained by the Gibbs free energy formula, ΔG = ΔH-ΔS × T, and ΔG is a negative number.

When the protein is positively charged and the DNA is negatively charged, the process of electrostatic adsorption leading to the binding of the two reactants is actually an exothermic reaction [34]. This reaction

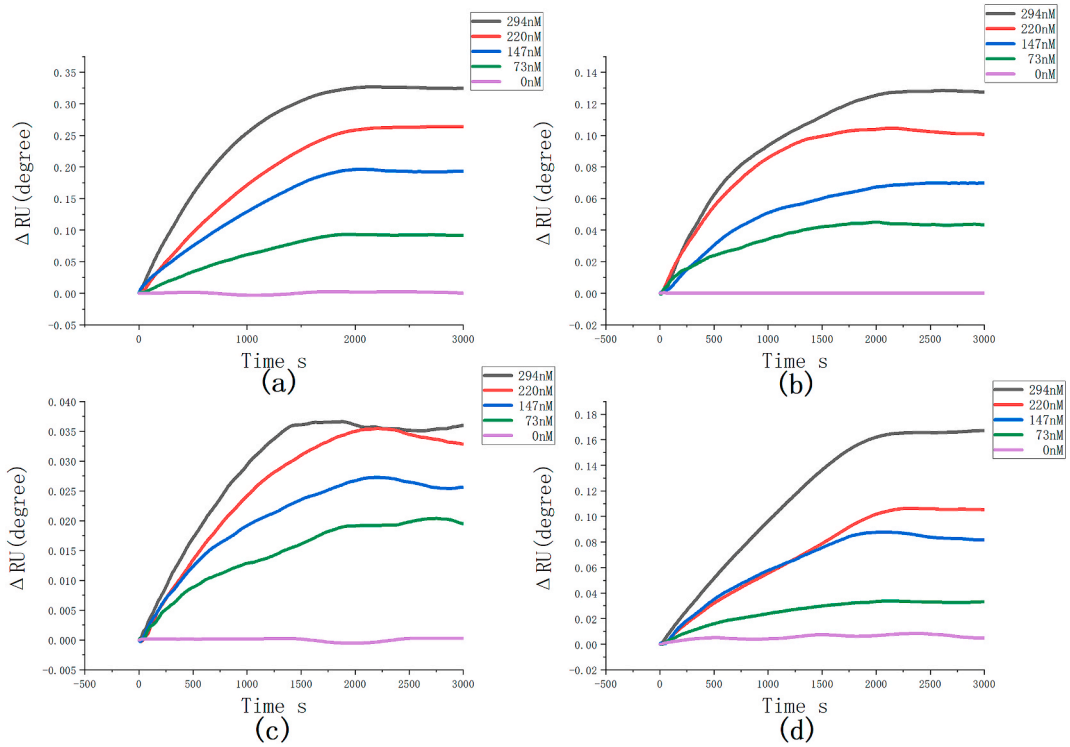

Fig. 5. SPR measurement results of 4 different HbA1c concentrations(aptamer0): (a) 0.1 M PB, pH = 6, (b) 0.1 M PB, pH = 6.96,(c) 0.1 M PB+137 mM NaCl, pH = 7.4, and (d) 0.1 M PB, pH = 7.4.

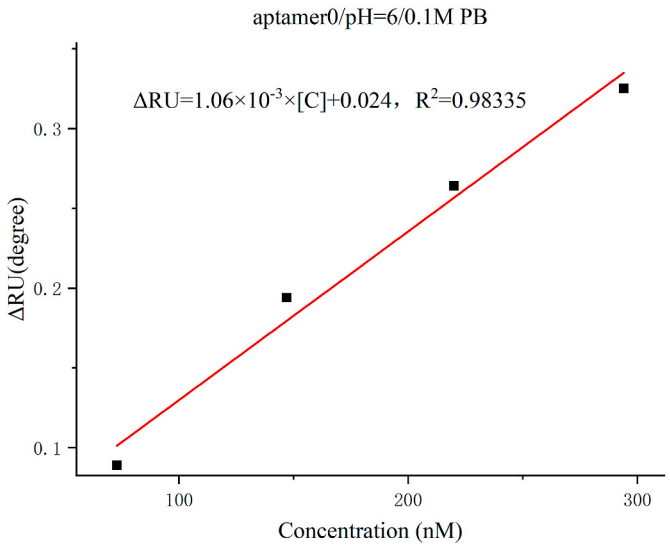

Fig. 6. Calibration lines of condition aptamer0/pH = 6/0.1 M PB for detection of HbA1c.

Table 3
Kinetic parameters for the affinity interaction between HbA1c and aptamer in different buffers.

Aptamer	Solution	pH	ka (M^{-1} s^{-1})	kd (s^{-1})	KA (M^{-1})
aptamer0	0.1 M PB	7.4	8.78×10^4	7.80×10^{-4}	1.12×10^7
aptamer0	0.1 M PB	6.96	1.91×10^3	8.68×10^{-4}	2.20×10^6
aptamer0	0.1 M PB	6	2.61×10^3	1.89×10^{-4}	1.38×10^7
aptamer0	0.1 M PB+137 mM NaCl	7.4	2.67×10^3	4.67×10^{-4}	5.71×10^6
aptamer1	0.1 M PB	7.4	1.72×10^4	2.87×10^{-3}	5.99×10^6
aptamer2	0.1 M PB	7.4	4.26×10^3	5.24×10^{-4}	8.13×10^6
aptamer3	0.1 M PB	7.4	3.53×10^3	5.31×10^{-4}	6.60×10^6

will have a large enthalpy reduction [35], and the entropy value (ΔS) will increase slightly at the same time (the heat released will increase the disorder). From an independent system perspective, it is a spontaneous reaction dominated by electrostatic forces.

Therefore, in the binding environment at pH = 6, the kinetic parameters are mainly manifested in a decrease in k_d, which is 0.25 times that at pH = 7.4. This result is because the formed complex is not easily dissociated due to electrostatic adsorption. In addition, under the conditions of pH = 7.4 with salt (137 mM NaCl), kd is also reduced, and its value is 0.5 times that of the condition without salt. This outcome is likely because the added salt ions coat the protein, which weakens the electrostatic repulsion effects [36], thereby slowing the dissociation rate of the complex.

3.5.2. *Effect of hydrophobic forces*

When the protein appears uncharged, the electrostatic force is almost zero, so the main force of HbA1c binding to the aptamer becomes the hydrophobic force. Some studies have shown that hydrophobic interactions are important interactions between proteins and aptamers [37–41].

In the case of the isoelectric point (pH = 6.96), the total surface area of the protein after binding to the aptamer is smaller than the surface area when it is not bound, resulting in a portion of the water molecules that encapsulate the protein and the aptamer becoming free water. This situation leads to an increase in the overall disorder, so ΔS is positive [42]. Compared to the pH = 6 condition, at pH = 6.96, the kinetic parameter k_a is slightly smaller, k_d is slightly larger, and K_A is smaller.

3.5.3. *Effect of aptamer structure changes*

Stems and loops on the aptamer structure can affect the affinity of the aptamer for binding to the analyte, which has been widely demonstrated [36,43–51]. Many studies have used a method of intercepting the stem-loop structure to determine which part of the aptamer plays a key role. The aptamers used in this study were found to have three characteristic loops by mfold simulation of the secondary structure, and aptamer structures lacking each characteristic loop were designed and simulated according to the principle of base complementary pairing. We used three designed aptamers (Fig. S1) for comparison with the prototype to determine which loop had the greatest effect on the affinity of the aptamer for HbA1c. Compared with those of the control group aptamer0 (pH = 7.4/0.1 M PB), the sensitivity and LOD of aptamer 1 are on the same order of magnitude, and k_a and k_d are increased by 1 order of magnitude; the sensitivity of aptamer2 is decreased by 70%, the LOD is increased by 1 order of magnitude, k_a is reduced by 50% and k_d is reduced by approximately 25%; and the sensitivity of aptamer 3 is reduced by 80%, the LOD is increased by 1 order of magnitude, k_a is reduced by 60%, and k_d is reduced by approximately 25%. In terms of kinetic parameters, L1 may play an important role in accurately identifying HbA1c, which is mainly reflected by aptamer 1, which lacks the L1 loop, increasing the association rate and dissociation rate of the complex at the same time; L2 and L3 on the aptamer assist in adsorbing HbA1c, which is reflected in a large decrease in k_a and a small decrease in k_d. In view of the changes in k_a and k_d, it is concluded that among the three loops, L1 may be important to identify HbA1c.

4. Conclusion

The pH and the salt concentration can greatly affect the formation of a complex between an aptamer and HbA1c. In addition, loop L1 on the structure of the aptamer may be an important structure to recognize glycated hemoglobin. Furthermore, the interaction between the aptamer and HbA1c includes electrostatic and hydrophobic forces. The spontaneous reaction of the complex can be attributed to enthalpy-entropy compensation. Moreover, the best condition for detecting HbA1c was pH 6, with a high sensitivity and a low LOD. This work has demonstrated that SPR analysis can successfully detect and quantify the binding of HbA1c to an aptamer monolayer by specific interactions. This methodology may prove to be useful in clinical diagnosis and could serve as an aptamer assay for HbA1c binding ability.

Author contributions

Conceptualization, Shwu-Jen Chang, Ching-Jung Chen and Jen-Tsai Liu; Methodology, Dapeng Sun, Ching-Jung Chen and Jen-Tsai Liu; Experiments, Dapeng Sun: Validation, Dapeng Sun and Ching-Jung Chen; Formal analysis, Dapeng Sun and Jen-Tsai Liu; Data curation, Dapeng Sun and Jen-Tsai Liu; Writing—original draft preparation, Dapeng Sun, Yi Wu, Ching-Jung Chen and Jen-Tsai Liu; Writing—review and editing, Ching-Jung Chen and Jen-Tsai Liu; Supervision, Shwu-Jen Chang, Ching-Jung Chen and Jen-Tsai Liu; Project administration, Shwu-Jen Chang, Ching-Jung Chen and Jen-Tsai Liu; All authors have read and agreed to the published version of the manuscript.

Declaration of competing interest

The authors declare that they have no known competing financial interests or personal relationships that could have appeared to influence the work reported in this paper.

Acknowledgements

This work was supported by the UCAS Young teacher research fund (Y95401H).

Appendix A. Supplementary data

Supplementary data to this article can be found online at https://doi.org/10.1016/j.talanta.2020.121466.

References

[1] A.R. da Mata, J. Alvares, L.M. Diniz, M.R.R. da Silva, B.R.A. dos Santos, A. A. Guerra, M.L. Cherchiglia, E.I.G. Andrade, B. Godman, F.D. Acurcio, Quality of life of patients with diabetes mellitus types 1 and 2 from a referal health centre in minas gerais, Brazil, Expet Rev. Clin. Pharmacol. 9 (5) (2016) 739–746.
[2] A. Girach, D. Manner, M. Porta, Diabetic microvascular complications: can patients at risk be identified? A review, Int. J. Clin. Pract. 60 (11) (2006) 1471–1483.
[3] D.M. Nathan, P. McGee, M.W. Steffes, J.M. Lachin, D.E.R. Grp, Relationship of glycated albumin to blood glucose and HbA(1c) values and to retinopathy, nephropathy, and cardiovascular outcomes in the DCCT/EDIC study, Diabetes 63 (1) (2014) 282–290.
[4] J.T. Liu, L.Y. Chen, M.C. Shih, Y. Chang, W.Y. Chen, The investigation of recognition interaction between phenylboronate monolayer and glycated hemoglobin using surface plasmon resonance, Anal. Biochem. 375 (1) (2008) 90–96.
[5] C. Weykamp, HbA1c: a review of analytical and clinical aspects, Ann. Lab. Med. 33 (6) (2013) 393–400.
[6] S.C.B. Gopinath, T. Lakshmipriya, Y. Chen, W.M. Phang, U. Hashim, Aptamer-based 'point-of-care testing', Biotechnol. Adv. 34 (3) (2016) 198–208.
[7] H.I. Lin, C.C. Wu, C.H. Yang, K.W. Chang, G.B. Lee, S.C. Shiesh, Selection of aptamers specific for glycated hemoglobin and total hemoglobin using on-chip SELEX, Lab Chip 15 (2) (2015) 486–494.
[8] M. Kimoto, R. Yamashige, K. Matsunaga, S. Yokoyama, I. Hirao, Generation of high-affinity DNA aptamers using an expanded genetic alphabet, Nat. Biotechnol. 31 (5) (2013) 453–+.
[9] J. Homola, S.S. Yee, G. Gauglitz, Surface plasmon resonance sensors: review, Sensor. Actuator. B Chem. 54 (1–2) (1999) 3–15.
[10] X. He, L. Guo, J. He, H. Xu, J. Xie, Stepping library-based post-SELEX strategy approaching to the minimized aptamer in SPR, Anal. Chem. 89 (12) (2017) 6559–6566.
[11] S. Wang, Y. Dong, X. Liang, Development of a SPR aptasensor containing oriented aptamer for direct capture and detection of tetracycline in multiple honey samples, Biosens. Bioelectron. 109 (2018) 1–7.
[12] A. Wochner, M. Menger, D. Orgel, B. Cech, M. Rimmele, V.A. Erdmann, J. Glökler, A DNA aptamer with high affinity and specificity for therapeutic anthracyclines, Anal. Biochem. 373 (1) (2008) 34–42.
[13] K.W. Chang, J. Li, C.H. Yang, S.C. Shiesh, G.B. Lee, An integrated microfluidic system for measurement of glycated hemoglobin levels by using an aptamer-antibody assay on magnetic beads, Biosens. Bioelectron. 68 (2015) 397–403.
[14] S. Eissa, M. Zourob, Aptamer-based label-free electrochemical biosensor array for the detection of total and glycated hemoglobin in human whole blood, Sci. Rep. 7 (2017) 8.
[15] J. Li, K.W. Chang, C.H. Wang, C.H. Yang, S.C. Shiesh, G.B. Lee, On-chip, aptamer-based sandwich assay for detection of glycated hemoglobins via magnetic beads, Biosens. Bioelectron. 79 (2016) 887–893.
[16] A. Davydova, M. Vorobyeva, E. Bashmakova, P. Vorobjev, O. Krasheninina, A. Tupikin, M. Kabilov, V. Krasitskaya, L. Frank, A. Venyaminova, Development and characterization of novel 2'-F-RNA aptamers specific to human total and glycated hemoglobins, Anal. Biochem. 570 (2019) 43–50.
[17] L.S. John Ho, R. Fogel, J.L. Limson, Generation and screening of histamine-specific aptamers for application in a novel impedimetric aptamer-based sensor, Talanta 208 (2020) 120474.
[18] V. Singh, R. Nerimetla, M. Yang, S. Krishnan, Magnetite-quantum dot immunoarray for plasmon-coupled-fluorescence imaging of blood insulin and glycated hemoglobin, ACS Sens. 2 (7) (2017) 909–915.
[19] D. Koval, V. Kasicka, H. Cottet, Analysis of glycated hemoglobin A1c by capillary electrophoresis and capillary isoelectric focusing, Anal. Biochem. 413 (1) (2011) 8–15.
[20] C.G. Zhang, S.J. Chang, K. Settu, C.J. Chen, J.T. Liu, High-sensitivity glycated hemoglobin (HbA1c) aptasensor in rapid-prototyping surface plasmon resonance, Sensor. Actuator. B Chem. 279 (2019) 267–273.
[21] M. Zuker, Mfold web server for nucleic acid folding and hybridization prediction, Nucleic Acids Res. 31 (13) (2003) 3406–3415.
[22] S. Chen, L. Li, C.L. Boozer, S. Jiang, Controlled chemical and structural properties of mixed self-assembled monolayers of alkanethiols on Au(111), Langmuir 16 (24) (2000) 9287–9293.
[23] C. Rodriguez Emmenegger, E. Brynda, T. Riedel, Z. Sedlakova, M. Houska, A. B. Alles, Interaction of blood plasma with antifouling surfaces, Langmuir 25 (11) (2009) 6328–6333.
[24] Z.-W. Dai, L.-S. Wan, Z.-K. Xu, Surface glycosylation of polyacrylonitrile ultrafiltration membrane to improve its anti-fouling performance, J. Membr. Sci. 325 (1) (2008) 479–485.
[25] H. Wang, J. Ren, A. Hlaing, M. Yan, Fabrication and anti-fouling properties of photochemically and thermally immobilized poly(ethylene oxide) and low molecular weight poly(ethylene glycol) thin films, J. Colloid Interface Sci. 354 (1) (2011) 160–167.
[26] L.J. Zhu, L.P. Zhu, Y.F. Zhao, B.K. Zhu, Y.Y. Xu, Anti-fouling and anti-bacterial polyethersulfone membranes quaternized from the additive of poly(2-dimethylamino ethyl methacrylate) grafted SiO2 nanoparticles, J. Mater. Chem. 2 (37) (2014) 15566–15574.
[27] A.R. MacDairmid, M.C. Gallagher, J.T. Banks, Structure of dithiothreitol monolayers on Au(111), J. Phys. Chem. B 107 (36) (2003) 9789–9792.
[28] G.K. Toworfe, R.J. Composto, I.M. Shapiro, P. Ducheyne, Nucleation and growth of calcium phosphate on amine-, carboxyl- and hydroxyl-silane self-assembled monolayers, Biomaterials 27 (4) (2006) 631–642.
[29] G.X. Wang, X.L. Su, Q.J. Xu, G.Y. Xu, J.H. Lin, X.L. Luo, Antifouling aptasensor for the detection of adenosine triphosphate in biological media based on mixed self-assembled aptamer and zwitterionic peptide, Biosens. Bioelectron 101 (2018) 129–134.
[30] P. Actis, A. Rogers, J. Nivala, B. Vilozny, R.A. Seger, O. Jejelowo, N. Pourmand, Reversible thrombin detection by aptamer functionalized STING sensors, Biosens. Bioelectron. 26 (11) (2011) 4503–4507.
[31] K. Chang, J. Li, C. Yang, S. Shiesh, G. Lee, Measurement of glycated hemoglobin using an aptamer/antibody assay on an integrated microfluidic system, in: The 9th IEEE International Conference on Nano/Micro Engineered and Molecular Systems (NEMS), 2014, pp. 647–650.
[32] K.-W. Chang, J. Li, C.-H. Yang, S.-C. Shiesh, G.-B. Lee, An integrated microfluidic system for measurement of glycated hemoglobin Levels by using an aptamer–antibody assay on magnetic beads, Biosens. Bioelectron. 68 (2015) 397–403.
[33] J.-M. Moon, D.-M. Kim, M.H. Kim, J.-Y. Han, D.-K. Jung, Y.-B. Shim, A disposable amperometric dual-sensor for the detection of hemoglobin and glycated hemoglobin in a finger prick blood sample, Biosens. Bioelectron. 91 (2017) 128–135.
[34] Y. Li, G. Ran, G. Lu, X. Ni, D. Liu, J. Sun, C. Xie, D. Yao, W. Bai, Highly sensitive label-free electrochemical aptasensor based on screen-printed electrode for detection of cadmium (II) ions, J. Electrochem. Soc. 166 (6) (2019) B449–B455.
[35] S. Zhang, F.-X. Li, J.-y. Yu, Y.-L. Hsieh, Dissolution behaviour and solubility of cellulose in NaOH complex solution, Carbohydr. Polym. 81 (3) (2010) 668–674.
[36] T. Hianik, V. Ostatná, M. Sonlajtnerova, I. Grman, Influence of ionic strength, pH and aptamer configuration for binding affinity to thrombin, Bioelectrochemistry 70 (1) (2007) 127–133.
[37] Y. Xu, L. Yang, X. Ye, P. He, Y. Fang, in: An Aptamer-Based Protein Biosensor by Detecting the Amplified Impedance Signal, vol. 18, 2006, pp. 1449–1456, 15.
[38] P.-H. Lin, R.-H. Chen, C.-H. Lee, Y. Chang, C.-S. Chen, W.-Y. Chen, Studies of the binding mechanism between aptamers and thrombin by circular dichroism, surface plasmon resonance and isothermal titration calorimetry, Colloids Surf. B Biointerfaces 88 (2) (2011) 552–558.
[39] Y.-H. Lao, K.K.L. Phua, K.W. Leong, Aptamer nanomedicine for cancer therapeutics: barriers and potential for translation, ACS Nano 9 (3) (2015) 2235–2254.
[40] A.D. Gelinas, D.R. Davies, N. Janjic, Embracing proteins: structural themes in aptamer–protein complexes, Curr. Opin. Struct. Biol. 36 (2016) 122–132.
[41] H. Hasegawa, N. Savory, K. Abe, K. Ikebukuro, in: Methods for Improving Aptamer Binding Affinity, vol. 21, 2016, p. 421, 4.
[42] C. Molitor, A. Bijelic, A. Rompel, The potential of hexatungstotellurate (VI) to induce a significant entropic gain during protein crystallization, Iucrj 4 (2017) 734–740.
[43] E.-i. Fukusaki, T. Kato, H. Maeda, N. Kawazoe, Y. Ito, A. Okazawa, S.-i. Kajiyama, A. Kobayashi, DNA aptamers that bind to chitin, Bioorg. Med. Chem. Lett 10 (5) (2000) 423–425.
[44] T. Kato, T. Takemura, K. Yano, K. Ikebukuro, I. Karube, In vitro selection of DNA aptamers which bind to cholic acid, Biochim. Biophys. Acta Gene Struct. Expr. 1493 (1) (2000) 12–18.
[45] O.Y. Yakimovich, Y.I. Alekseev, A.V. Maksimenko, O.L. Voronina, V.G.J.B. Lunin, in: Influence of DNA aptamer structure on the specificity of binding to Taq DNA Polymerase, vol. 68, 2003, pp. 228–235, 2.
[46] J. Tang, J. Xie, N. Shao, Y. Yan, in: The DNA aptamers that specifically recognize ricin toxin are selected by two in vitro selection methods, vol. 27, 2006, pp. 1303–1311, 7.
[47] D. Shangguan, Z. Tang, P. Mallikaratchy, Z. Xiao, W. Tan, in: Optimization and modifications of aptamers selected from live cancer cell lines, vol. 8, 2007, pp. 603–606, 6.
[48] X.J. Yang, T. Bing, H.C. Mei, C.L. Fang, Z.H. Cao, D.H. Shangguan, Characterization and application of a DNA aptamer binding to L-tryptophan, Analyst 136 (3) (2011) 577–585.
[49] M. Svobodová, V. Skouridou, M.L. Botero, M. Jauset-Rubio, T. Schubert, A. S. Bashammakh, M.S. El-Shahawi, A.O. Alyoubi, C.K. O'Sullivan, The characterization and validation of 17β-estradiol binding aptamers, J. Steroid Biochem. Mol. Biol. 167 (2017) 14–22.
[50] Y. Wang, Z. Fang, G. Ning, S. Mao, Y. Wu, S. Wu, G.-Q. Liu, G-quadruplex-bridged triple-helix aptamer probe strategy: a label-free chemiluminescence biosensor for ochratoxin A, Sensor. Actuator. B Chem. 298 (2019) 126867.
[51] Y. Zhang, G. Figueroa-Miranda, C. Zafiu, D. Willbold, A. Offenhäusser, D. Mayer, Amperometric aptasensor for amyloid-β oligomer detection by optimized stem-

loop structures with an adjustable detection range, ACS Sens. 4 (11) (2019) 3042–3050.